electronics

MDPI

Article

Simulation of a Line Voltage Regulator in a Low-Voltage Grid That Is Subject to Strong Voltage Surges Due to the Provision of Fast Frequency Reserve

Maximilian Hauschel [1] and Kent Bertilsson [2,*]

[1] University of Applied Forest Sciences Rottenburg, 72108 Rottenburg, Germany; maximilian.hauschel@student-hfr.de
[2] STC Research Centre, Department of Computer and Electrical Engineering, Mid-Sweden University, 851 70 Sundsvall, Sweden
* Correspondence: kent.bertilsson@miun.se

Abstract: The increasing adoption of battery storage units alongside private PV systems may prove to be a new challenge for distribution grid operators. This study explored the potential impact of marketing aggregated battery discharge power as a Fast Frequency Reserve (FFR) and its effect on the distribution grid stability. We investigated the efficacy of Line Voltage Regulators (LVRs) in mitigating voltage surges caused by simultaneous battery activation. For this purpose, a simulation was developed via Matlab (Version R2023a) to simulate the voltage at the nodes of an arbitrary distribution grid, using the feed-in and consumed power of the customers as the input. We applied the model to a distribution grid section in Sundsvall (Sweden). The results confirmed that LVRs can amplify voltage surges when their adjustments are not synchronized with the FFR activation. This study underscored the need for proactive measures to address the voltage maintenance challenges arising from the integration of battery storage units and renewable energy sources.

Keywords: line voltage regulator; ancillary services; fast frequency reserve; distribution grid

check for updates

Citation: Hauschel, M.; Bertilsson, K. Simulation of a Line Voltage Regulator in a Low-Voltage Grid That Is Subject to Strong Voltage Surges Due to the Provision of Fast Frequency Reserve. *Electronics* **2024**, *13*, 2363. https://doi.org/10.3390/electronics13122363

Academic Editor: Rui Castro

Received: 9 April 2024
Revised: 31 May 2024
Accepted: 1 June 2024
Published: 17 June 2024

Copyright: © 2024 by the authors. Licensee MDPI, Basel, Switzerland. This article is an open access article distributed under the terms and conditions of the Creative Commons Attribution (CC BY) license (https://creativecommons.org/licenses/by/4.0/).

1. Introduction

The increasing integration of local renewable energies into low-voltage grids poses a new challenge for grid stability [1]. Low-voltage grids were originally designed to receive electrical energy from a higher voltage level and distribute it to the customers. The main challenge, which arises particularly from the growing number of private PV systems, is the decentralized reception and redistribution of the electricity generated from renewable sources. Decentralized feed-in can lead to strong voltage surges along a power line, which may cause damage to grid-connected devices. To avoid this, distribution system operators can shut down power plants or limit their feed-in [2]. Private battery storages can counteract this problem by absorbing the PV energy at peak times and releasing it to the grid later [3]. This flattens the sharp voltage spikes during high irradiation, which can prevent the associated shutdowns.

However, it is conceivable that in near future, private battery storage operators may aggregate their storage discharge capacities via an aggregator to offer them as a Fast Frequency Reserve (FFR) in the balancing power market. A techno-economic assessment has already shown that the profitability of PV household prosumers can be significantly improved by the provision of the frequency containment reserve (the analog to the FFR in the continental European grid) [4]. The simultaneous activation of aggregated capacities could, in turn, cause problems with the local voltage maintenance. It is assumed that at times of high local irradiation, the utility frequency-controlled activation of the FFR poses a risk of overvoltages in the distribution grid.

To identify overvoltages, a reference voltage (V_{ref}) is required, to which the actual values of the voltage can be related. In Swedish low-voltage networks, the V_{ref} is 230 V and thus corresponds to the effective value of the phase-to-ground voltage [5]. Significant deviations from the V_{ref} can cause severe damage to the electrical equipment and machinery [6]. Therefore, it is necessary to keep the voltage within the tolerance range. The legal requirement for slow voltage changes is that the deviation of the 10-min average rms values of the mains voltage must not exceed ±10% of the V_{ref} [7]. For short-term voltage changes, where the rms value of the voltage deviates from the V_{ref} by more than 10% by definition, special requirements apply depending on the duration of the voltage change. Investigated in this work were the effects of short-term voltage increases. If their duration is between 0.2 and 5 s, the measured voltages must be smaller than 135% of the V_{ref}. For voltage increases with a duration of more than 5 s and up to a maximum of 60 s, the voltages must be below 115% of the V_{ref} [7].

A line voltage regulator (LVR) can prove to be a suitable countermeasure for the voltage deviations in a distribution grid, especially if they occur in long branches. It is a component for regulating the voltage of a line, by injecting a control voltage via a series of transformers [8]. The LVR is positioned at a specific point in the grid where it enables both an increase and a decrease of the phase-to-ground voltage of each phase. The phase-to-ground voltage will simply be referred to as the "voltage" in the following. The voltage adjustment affects all the downstream line sections.

Figure 1 shows both the voltage reduction (a) and the voltage increase (b) by the LVR to keep the line voltage within the tolerance range. In this example, the tolerance range is limited by the maximum and minimum rms values of the voltage for the slow voltage changes. The voltage is plotted on the *y*-axis, while the *x*-axis describes the distance to the transformer. Without the activation of the LVR, the voltage would break out of the tolerance range in both scenarios (dotted lines). In this example, the LVR can keep the voltage within the tolerance range; however, the gradual voltage adjustment by the LVR leads to rapid voltage changes and can therefore cause flicker effects [9]. Further problems could be caused by the delay in the voltage adjustment, which is an inherent part of the control algorithms of LVRs with tap changers [10]. It is suspected that the LVR could amplify voltage surges due to this delayed response.

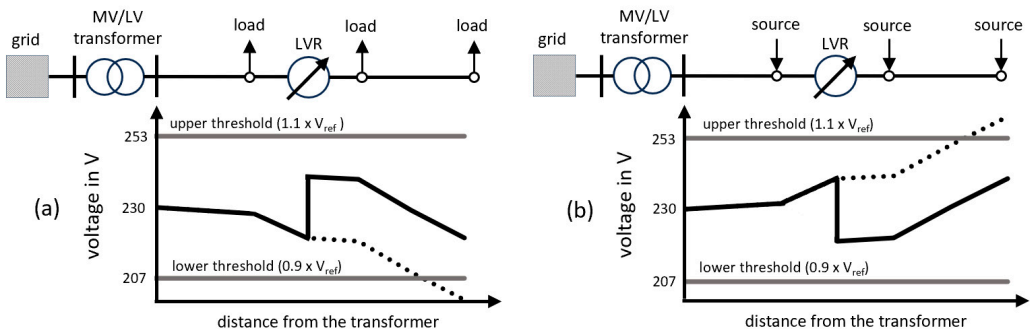


Figure 1. LVR operation in the case of impending undervoltage (**a**) and overvoltage (**b**). Source: [11].

The aim of this work was to check, in different scenarios, whether the LVR can keep the line voltage within the permitted tolerance range or not. Furthermore, the hypothesis was tested as to whether the LVR can amplify the voltage surges in its current mode of operation. It was also investigated to what extent the position of the LVR in the grid affects its effectiveness. To accomplish these tasks, a model was developed to simulate the voltages occurring in an arbitrary distribution grid, accounting for the varying behaviors in customer feed-in and consumption. The model was applied to a network section of the Swedish grid operator, Sundsvall elnät, where an LVR regulates the voltage in one of the three main lines leading from the transformer.

The results confirmed the hypothesis that the LVR can amplify the voltage surges after the FFR activation. This occurred when the LVR increased the voltage before the FFR

activation started and did not immediately switch to the voltage reduction. Furthermore, the simulation results showed that a voltage violation may occur if the FFR activation coincides with a high PV injection. In such cases, the voltage reduction by the LVR was not sufficient.

Distribution system operators need to prepare for these scenarios to be resilient to future voltage maintenance challenges. To avoid an amplification of the voltage surges, the distribution system operator could adjust the operation of the LVR during the standby period of the FFR capacities. This would require communication between the distribution system operator and the aggregator.

2. Functioning of the LVR

LVRs basically use the principle of electromagnetic induction feeding in $\pm\Delta V$ in a series transformer, even though the devices from different manufacturers differ in terms of their design. Depending on the design, the induction voltage can be adjusted in steps or continuously [11]. The LVR considered in this paper was from Hitachi Energy (Zurich, Switzerland) and was specially designed for low-voltage grids. It regulates the volage stepwise using a tap changer. The detailed working mechanism is explained in the following sections.

The voltage is changed phase-specifically by a booster transformer, the secondary coil of which is integrated into the respective phase. This enables the input voltage V_a to be raised or lowered to the output voltage V_b, which can be seen in Figure 2. The booster transformer is fed by a feeder transformer, the primary coil of which is connected to the outer conductor. To enable the induction, a control current must be supplied to or removed from it. An increase in the voltage is therefore always accompanied by a decrease in the current and a decrease in the voltage by an increase in the current. On the secondary side of the feeder transformer, there is a tap changer for the stepwise regulation of the induced voltage that causes the inductor current, which in turn causes the induction at the booster transformer. Through this mechanism, a stepwise change in the voltage can be made from -8% to $+8\%$ of the input voltage V_a. The step size is 1.6% of the input voltage, giving a total of 11 taps controlled by five contactors (S1–S5) [12]. By means of four additional contactors (K1–K4), the booster transformer can be reversed, thus allowing the bidirectional voltage changes. All the information on the LVR's working mechanism that is not included in the data sheet was provided by Sundsvall elnät.

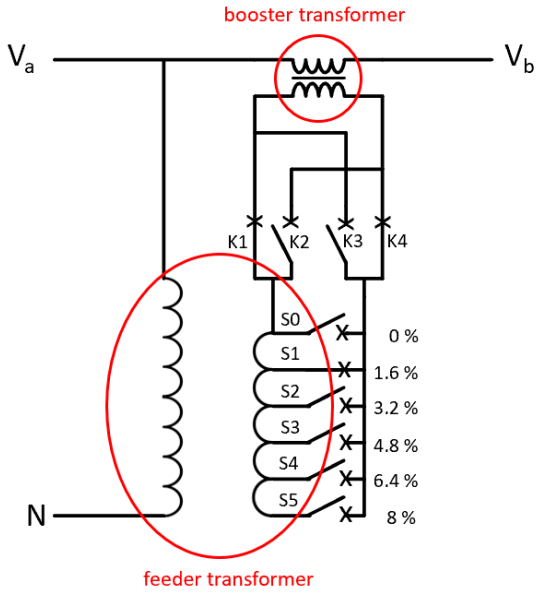


Figure 2. Circuit diagram of the LVR, provided by Sundsvall elnät and modified.

The control of the voltage regulation works as follows: at the installation location of the LVR, its input voltage V_a is recorded. To predict the voltage deviation at the end of the line in which the LVR is used—this is where the greatest deviations are to be expected—Sundsvall elnät uses an algorithm, which has not been provided to us. Therefore, to predict the voltage at the end of the line, a function was created, which is further explained on pages 10 and 11. In the case of a tap change, the tap that brings the assumed voltage at the end of the line closest to the reference voltage is selected.

Since the too-frequent clocking of the LVR leads to increased wear, a delay is implemented in the control algorithm of the tap changers, which prevents the LVR from being triggered if the voltage leaves the allowed range for only a very short time. The delay works as follows: If the voltage exceeds or falls below a certain threshold value, a timer is started. If the voltage returns to the allowed deadband before the set delay has elapsed, then no tap change occurs. Otherwise, a tap change takes place to return the voltage to the tolerance range [10]. For the implementation in the simulation, a tap change is initiated as soon as the mentioned conditions are fulfilled by the voltage that is predicted at the end of the line. The set tolerance range is $V_{ref} \pm 0.1\ V_{ref}$, which corresponds to the threshold value of short-term voltage deviations.

We set the delay to 5 s, as we assumed that this corresponded to the current control setting of the LVR used by Sundsvall elnät. Furthermore, we assumed the delay to be adjustable in some intervals. A comparative study from 2014 showed that the time delays of tenths of a second to a few minutes can be set for the control algorithms of the established tap changers [10]. In general, a shorter delay is expected to result in more precise control and fewer voltage maintenance problems. However, we considered a delay shorter than 5 s to be unlikely, as this could lead to a more sensitive reaction of the LVR to short-term voltage fluctuations. The resulting more-frequent voltage adjustments would lead to a higher wear and tear.

The delay is a central assumption for this work because it may prove to be problematic in the case of short-term events, such as an FFR activation. The expected problem is the following: If there is an undervoltage before the FFR activation, which is compensated by the LVR, the voltage boost remains active until the next tap change. However, if the FFR activation occurs before the next tap change, the voltage will increase rapidly, while the LVR continues to boost it. In this case, the LVR could amplify the voltage surges, thereby increasing the likelihood of exceeding the permitted voltage limits. The delay has a significant influence on the duration of the exceedance, as it determines the minimum time interval between two tap changes.

Another key assumption is the starting tap of the tap changer. This depends on which events occurred in the grid before the simulation and how the LVR reacted to them. Consequently, an assumption must be made. In the simulation, the tap changer always takes the initial position at which the voltage at the end of the line shows the smallest deviation. The reason for this is that this setting is considered to be the most stable during normal grid operation. In situations with rapid voltage changes, such as an FFR activation, however, this may be different. For example, if a voltage boost ensures a stable grid situation during normal operation, a sudden voltage increase is more likely to lead to overvoltages, as long as the additional voltage boost is still active. The chosen start setting could therefore lead to greater voltage deviations in the simulation than if a different tap was used as the start setting.

Figure 3 shows a flow diagram of the assumed control process of the LVR, specific to the considered application of Sundsvall elnät. In other cases, the first two steps can be replaced, for example, by a direct measurement at the node of interest, in this case at the end of the line, and use the measured value there as a control variable.

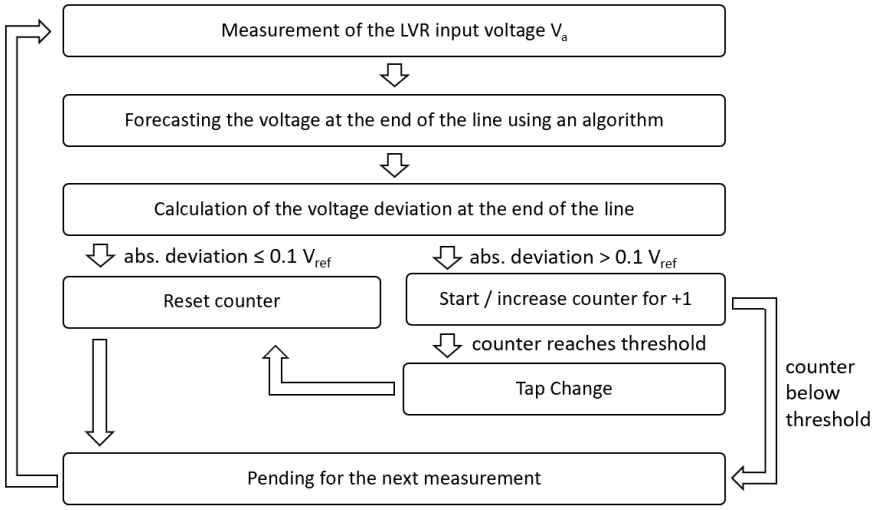


Figure 3. Grid with the transformer station and the LVR-Group.

3. Modelling of the Low-Voltage Grid and the Prosumers

3.1. Modelling of the Low-Voltage Grid

Figure 4 shows the examined grid section of the grid operator Sundsvall elnät. In total, 49 customers were connected to the grid. It consisted of several lines of different lengths, which were made up of line sections. The start and end points of these line sections represent the nodes of the respective lines and are each marked with an individual six- to seven-digit identification number. In the center, there was the transformer from which the busbar (black line section) started. The transformer has the identification number 0. In the line extending from the transformer to the top left, the LVR was installed. The LVR group included all customers that were directly or indirectly connected to this line, totaling 17. For better clarity, the nodes of this line were additionally numerated from 1 to 13.

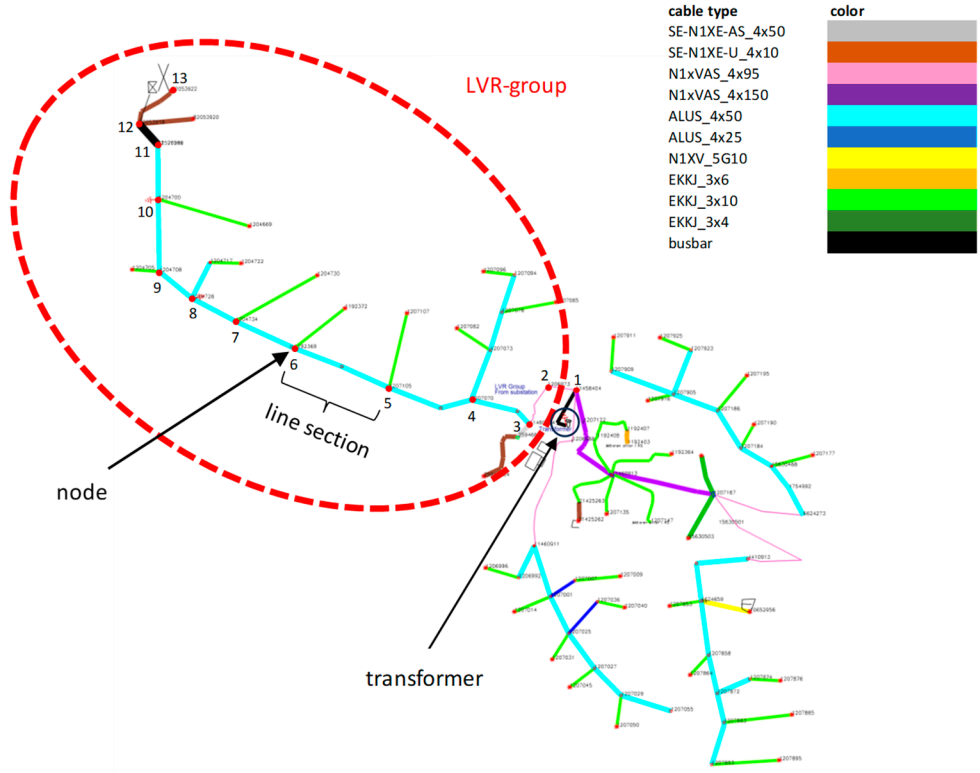


Figure 4. Grid with the transformer station and the LVR-Group. Source: Sundsvall elnät.

To model the grid section, it needed to be systematized. For this purpose, the lines of the grid needed to be defined. A line was defined as a continuous connection of the line sections that ended at the connection point of a consumer. To define the initial node (entry point) of each line, a two-dimensional array *EP* with two columns was created. The number of lines corresponded to the number of rows, giving each line an individual row index *k*.

The first column *EP*(*k*,1) contained the row index of the upstream line, from which the line *k* originated. If the line had its origin at the transformer, the value corresponded to its own row index. The second column *EP*(*k*,2) contained the number of the node *n* of the upstream line to which the line was connected. If a line was connected directly to the transformer, this value was 0. Table 1 and Figure 5 belong together and illustrate this principle. Line 1 started from the transformer and therefore took the value of its row index *k* in the first column and the value of 0 in the second column. Line 2 originated from line 1 and was connected to its first node. Therefore, *EP*(2,1) and *EP*(2,2) both took the value 1. For the third line, which started at the first node of the second line, *EP*(3,1) took the value of 2 and *EP*(3,2) took the value of 1.

Table 1. Array EP for defining the line entry points.

k	*EP*(*k*,1)	*EP*(*k*,2)
1	1	0
2	1	1
3	2	1

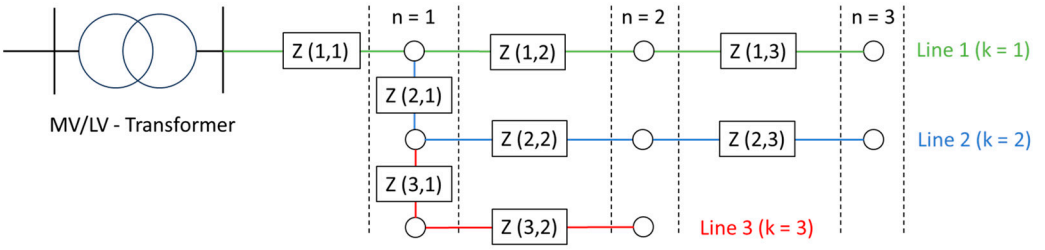


Figure 5. Exemplary grid to illustrate the defined lines and their entry points.

The line sections, i.e., connections of two nodes, had different impedances depending on the cable type used (color-coded in Figure 4) and its respective length. The single-phase impedances were provided by Sundsvall elnät for this work. The values of the impedances were saved in the array *Z*(*k*,*n*). In this array, each line again had the specific row index *k*. The columns contained the impedances of the line sections belonging to the respective line. The column index *n* corresponded to the number of the node at which the line section ended. The number of nodes of the longest line thus specified the total number of columns *N* of the array. For the lines with less than *N* nodes, which had less than *N* line segments correspondingly, the column values that could not be associated with a line segment were assigned the value 0 Ω. This can be observed for *Z*(3,3) in Table 2, which contains the impedances associated with Figure 6.

Table 2. Array *Z*(*k*,*n*) with the single-phase impedances of the line segments.

k	*Z*(*k*,1) in Ω	*Z*(*k*,2) in Ω	*Z*(*k*,3) in Ω
1	0.05	0.04	0.04
2	0.02	0.03	0.05
3	0.01	0.01	0

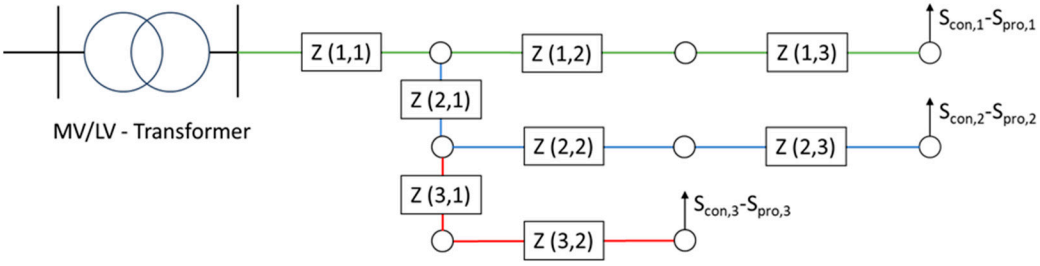


Figure 6. Exemplary grid with the apparent power balance of the prosumers.

3.2. Modelling of the Prosumers

The nodes at which the lines ended were the connection points between the customers and the grid. Since the customers both consumed and generated electrical energy, they were referred to as prosumers. Consequently, they could deliver the electrical power to the grid and receive the electrical power from the grid. The apparent power fed into or taken from the grid at each connection point depended on the power balance of the prosumers connected to it. This is illustrated on the right-hand side of the figure below.

$S_{\mathrm{con,k}}$ was the apparent power consumed by the prosumers at the last node of line k, whereas $S_{\mathrm{pro,k}}$ corresponded to the apparent power delivered there. The difference between the two values was the apparent power balance S_{k} drawn from or delivered to the grid at the connection point. Since the prosumers were residential customers with multiple electrical loads, $S_{\mathrm{con,k}}$ represented the summed apparent power consumption of all their loads. A power output can be caused by photovoltaic systems, as well as by battery storages. The resulting equation for the power balance of the customers at the connection point of line k is shown below. In this equation, $S_{\mathrm{pv,k}}$ corresponds to the apparent power output of the PV systems and $S_{\mathrm{bat,k}}$ to the apparent power output of the batteries.

$$S_k = S_{con,k} - S_{pro,k} = S_{con,k} - S_{pv,k} - S_{bat,k} \quad (1)$$

For the prosumers, the assumption was made that the power drawn from or delivered to the grid was evenly distributed across all three phases. Although the electrical loads in private households were generally only connected to one phase, the loads were ideally distributed as evenly as possible among the three phases, in order to avoid the asymmetrical loading of the phases [13]. Consequently, an even power draw from all the phases was an idealized assumption. In the case of the PV systems and batteries, on the other hand, the distribution of power to the phases depended on whether a three-phase or one-phase inverter was used. We made the idealized assumption that all the PV systems fed symmetrically into the grid via a three-phase inverter. The apparent power delivered or drawn by each prosumer was therefore identical in all three phases and was calculated as three times the string power. This was expressed using the following equation:

$$S_k = 3 \cdot S_{Str,k} = 3 \cdot V_{Str,k} \cdot I_k \quad (2)$$

where $V_{\mathrm{Str,k}}$ is the phase voltage and I_{k} is the phase current at the connection point of the line k. In the case of a star connection, which was used in this model, the string current and phase current are identical. For this reason, only the designation I_{k} is used instead of $I_{\mathrm{Str,k}}$. The current I_{k} was limited by the size of the fuses at the connection points, which were provided by Sundsvall elnät for this work. The absolute value of I_{k} could therefore only take values that were greater or equal to $I_{\mathrm{lim,k}}$.

4. Simulation of the Effective Voltages at the Nodes and Operation of the LVR

Considering the focus of this study on short-term voltage changes, a 60-s duration was selected for the total simulation period. The total duration, denoted as t, was divided into time steps of dt = 0.2 s each. At each time step, the process depicted in Figure 7 was

executed. Once the process for one time step was completed, the next time step began and the process repeated. The specific steps of the simulation process are explained below.

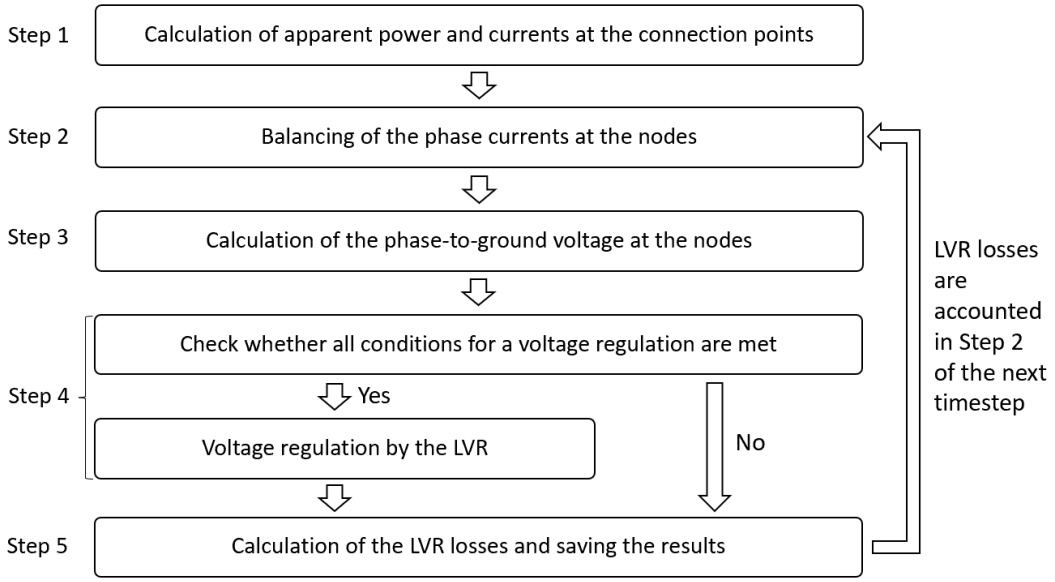


Figure 7. Flow chart of the calculation process for one time step *dt* with the duration of 0.2 s.

Step 1: In the first step, the apparent power and the phase currents at the connection points were calculated. As described in chapter 3.2, the apparent power for each connection point was calculated from the respective power balance. The values for $S_{\mathrm{con,k}}$, $S_{\mathrm{pv,k}}$, and $S_{\mathrm{bat,k}}$ depended on the scenarios under consideration, which will be defined in chapter 5. Following the calculation of the apparent power, the phase currents at the connection points were calculated. The phase current I_{k} at the connection point of line k was obtained using the transforming Equation (2) on the previous page, as follows:

$$I_k = \frac{S_k}{3 \cdot V_{Str,k}} \tag{3}$$

The string voltage $V_{\mathrm{Str,k}}$ corresponded to the phase-to-ground voltage, which deviated from the reference voltage V_{ref} depending on the distance to the transformer and the power balance of all the customers. In the first time step, the reference voltage was used to calculate the current at all the connection points. In the subsequent time steps, the local phase-to-ground voltage from the previous time step was used, which is calculated in steps 3 and 4.

Step 2: The second step covers the balance of the phase currents at the nodes of the grid. Neglecting the charge storage effects, at each node, the sum of all the incoming currents must be equal to the sum of all the outgoing currents. Starting from the connection points, the balance could be performed at all nodes. In this way, all the phase currents occurring in the grid were determined, as shown in Figure 8. The current ΔI_{LVR} required by the LVR, the calculation of which will be explained in step 5, was also considered when balancing the currents.

The designation of the currents in the line sections was based on the line index k and the node at which the line section ended, in the form $I(k,n)$. The direction of the arrows in Figure 8 depended on the sign of the current, which was identical to the sign of the apparent power. It indicated whether the prosumer drew electricity from the grid or fed it into the grid. For reasons of clarity, the line impedances are not shown in the diagram.

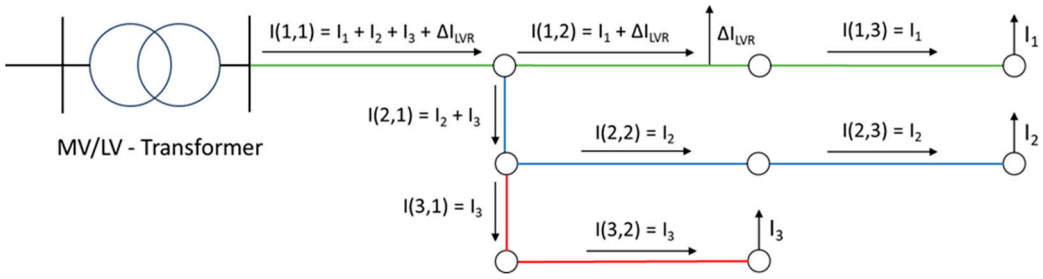


Figure 8. Exemplary grid to illustrate the calculation of the phase current in each line section.

Step 3: In the third step, the phase-to-ground voltage at each node of the grid was calculated. The voltage at node n of line k was designated as $V(k,n)$. To determine the voltage at the nodes, the voltage drop over each line section was first calculated from the phase current and the impedance of the line section. In the following equation, $\Delta V(k,n)$ represents the voltage drop of the line section in front of the node n of the line k.

$$\Delta V(k,n) = Z(k,n) \cdot I(k,n) \tag{4}$$

Then, starting from the phase-to-ground voltage applied to the transformer (V_0), the voltage at all nodes was determined successively. V_0 was assumed to be constant at 230 V. For the voltage at the first node of a line, which was directly connected to the transformer, the following equation applies:

$$V(k,1) = V_0 - \Delta V(k,1) \tag{5}$$

Whether a line started at the transformer or branched off from an upstream line was checked using the value $EP(k,2)$, defined in Section 3.1. If it was equal to 0, the line started at the transformer. In all the other cases, the line started at a node of an upstream line, where the row index of the upstream line could be identified by $EP(k,1)$ and the number of the node by $EP(k,2)$. For the voltage at the first node of a line not originating from the transformer, the following equation applies:

$$V(k,1) = V(EP(k,1), EP(k,2)) - \Delta V(k,1) \tag{6}$$

For all the other nodes after the initial node, the phase-to-ground voltage was calculated using the following equation:

$$V(k,n) = V(k,n-1) - \Delta V(k,n) \tag{7}$$

To ensure clarity, in Figure 9, the designations of the voltages, voltage drops, and line section impedances were annotated in the schematic of the exemplary grid.

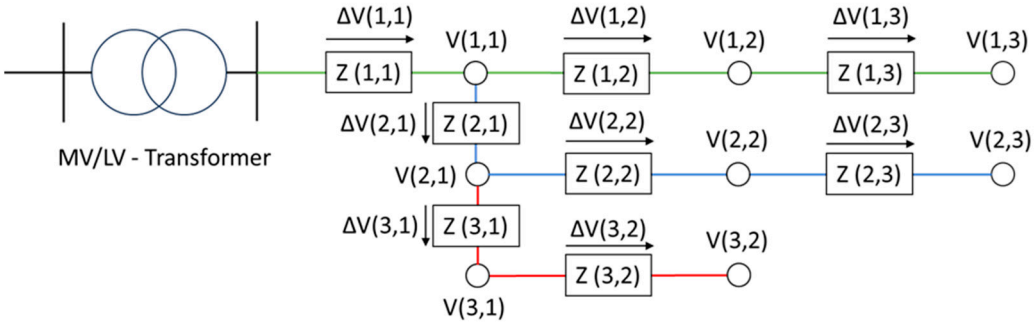


Figure 9. Designations of the voltages, voltage drops, and impedances in the exemplary grid.

Step 4: The fourth step dealt with the simulation of the voltage change caused by the LVR. An LVR that was installed in a specific line section was modeled between the impedance of that line section and the following node. The location of the LVR needed to be defined before starting the calculation process. This was calculated by specifying the two-dimensional vector $LVR_{pos} = (k_{LVR}, n_{LVR})$. Here, k_{LVR} corresponds to the line in which the LVR is installed and n_{LVR} corresponds to the node in front of which it is located. This is illustrated in Figure 10, where V_a is the input voltage and V_b the output voltage of the LVR.

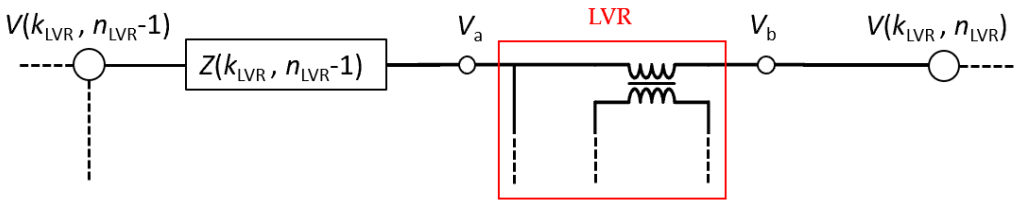


Figure 10. Positioning of the LVR in a power line, shown for one phase.

Using the voltage V_a as an input, an algorithm, which will be explained on the following pages, predicted the voltage at the end of the line. If there was a deviation of more than 10% from the reference voltage, a timestep counter was activated, which increased by +1 for each time step as long as the deviation was greater than 10%. Otherwise, the counter was reset. After each time step, a check was made to see whether the counter reached the threshold value *TH*. If this was the case, the LVR was triggered, and the counter was reset.

The threshold value of the counter was calculated, according to the Equation (8), from the quotient of t_{delay} and the duration of a time step dt. With the chosen delay of 5 s and the time step duration of 0.2 s, the threshold value equaled 25 time steps. This meant that if the counter reached the threshold value of 25, an activation of the LVR was triggered. An explanation on why the counter was implemented and a justification for the assumption of a five-second delay can be found in chapter 2 on page 4.

$$TH = \frac{t_{delay}}{dt} \tag{8}$$

Before the LVR was activated, both the V_a and V_b corresponded to the voltage at the node n_{LVR}. When the LVR was activated, a tap was set on the tap changer, which was maintained for the following 24 time steps. Depending on the selected tap, V_b took a value between −8% and +8% of the input voltage V_a. Using the taps, the voltage could be adjusted within this range in steps of 1.6%, resulting in a total of 11 steps [12]. Each tap was labeled with an index i, while $tap(i)$ was the associated percentage voltage adjustment. Equation (9) shows how the output voltage was calculated from the input voltage and the voltage change caused by the LVR. Equation (10) defines the absolute voltage change ΔV_{ab}, which was the product of V_a and $tap(i)$.

$$V_b = V_a \cdot (1 + tap(i)) \tag{9}$$

$$\Delta V_{ab} = V_a \cdot tap(i) \tag{10}$$

The aim of the voltage regulation was to achieve the smallest possible voltage deviation at the connection point of line k from the reference voltage V_{ref}. Consequently, the tap was selected by which the difference between the predicted voltage deviation at the connection point (ΔV_{set}) and the voltage change due to the LVR (ΔV_{ab}) assumed the smallest absolute value. Thus, if the absolute value of this difference was expressed by the function $f(i)$, the value for i at which the function had its minimum needed to be determined. The domain of the function comprised exclusively the natural numbers from 1 to 11, since only these represent a tap.

$$f(i) = |\Delta V_{ab} - \Delta V_{set}| = |V_a \cdot tap(i) - \Delta V_{set}| \tag{11}$$

$$f'(i) = 0 \tag{12}$$

$$f''(i) \geq 0 \tag{13}$$

To determine the minimum, a loop was used that calculated $f(i)$ for all the permissible values of i, sorted the results according to their magnitude, and selected the tap i that yielded the smallest result. The predicted voltage deviation at the connection point ΔV_{set} was determined based on the input voltage V_{a} and assuming a voltage drop or increase. Although ΔV_{set} could be calculated directly from the difference between the voltage at the connection point and the reference voltage V_{ref}, in the current operation, the LVR used only the local input voltage V_{a} as a control variable. The following section is therefore devoted to the determination of ΔV_{set}.

The starting point for the determination of ΔV_{set} was an observation that can be made for the investigated line k after the simulation ran without LVR: There exists a relationship between the ratio of the voltage deviation at the last node N to the voltage deviation at the node n and the number of nodes located between them. The ratio of the voltage deviations was expressed as follows:

$$\frac{V(k,\ N) - V_{ref}}{V(k,\ n) - V_{ref}} \tag{14}$$

The value of this ratio increased with the number of nodes between N and n, regardless of the sign of the voltage. When plotting this ratio over the difference between N and n in a 2-dimensional diagram and connecting the data points, an s-shaped curve became recognizable. To describe this relationship, a sigmoid function $g(x)$ was created in Matlab, using the Curve Fitter. The graph of the function was fitted to the data points resulting from simulating all scenarios when no LVR was used. The functional equation of the sigmoid function is shown below. Here, e is the Eulerian number and x is the independent variable that takes the difference of $N - n$. All the other coefficients resulted from the curve-fitting process and provided the sigmoid function its characteristics (a = 40.25, b = 4.102, c = 1.782, d = 10.46, h = 1.182).

$$g(x) = h + \frac{a}{b + e^{-(c \cdot (x-d))}} \tag{15}$$

The voltage deviation at the connection point could be predicted from the product of the function value and the voltage deviation at the node n:

$$V(k,N) - V_{ref} \approx g(x = N - n) \cdot \left(V(k,n) - V_{ref} \right) \tag{16}$$

If an LVR was positioned in front of the node n (n becomes n_{LVR}), the predicted voltage deviation at the connection point could be calculated by inserting the node n_{LVR} and the input voltage V_{a} into Equation (16). It was conclusive to insert the input voltage V_{a} for $V(k,n)$, as it corresponded to the voltage that would be present at the node n_{LVR} without the operation of the LVR. The resulting equation is shown below.

$$\Delta V_{set} = g(x = N - n_{LVR}) \cdot \left(V_a - V_{ref} \right) \tag{17}$$

This allowed the LVR to be set according to Equations (11) to (13), and to make the optimum voltage change. Due to the voltage change, the voltage $V(k_{\text{LVR}}, n_{\text{LVR}})$ took the value of the output voltage V_{b}. After the voltage at node n_{LVR} had changed, the voltage at all the subsequent nodes was recalculated by successively subtracting the voltage drops $\Delta V(k,n)$ determined in step 3.

The selected tap was maintained until the next LVR activation. Therefore, in the intervening time steps, the voltage $V(k_{\text{LVR}}, n_{\text{LVR}})$ was continuously changed by the tap, regardless of its value. The voltage applied to the subsequent nodes was again obtained by subtracting the voltage drops $\Delta V(k,n)$ determined in the current time step.

It should be noted that not every LVR activation resulted in a tap change. A tap remained active over multiple activations if it repeatedly resulted in the best approximation of the reference voltage V_{ref} at the end of the line.

Step 5: In the fifth and last step, the LVR losses were calculated and taken into account. It must not be neglected that part of the phase current was required by the LVR to enable the voltage boost. In the lossless operation, the apparent power, and thus the product of the voltage and phase current, would be the same before and after the LVR. Taking the losses into account, the apparent power after the LVR (S_{b}) must equal the product of the power before the LVR (S_{a}) and its efficiency. Since the efficiency was not known for all the taps, the minimum efficiency of 99.52% was used in all cases, as shown in the Equations (18) and (19).

$$S_a \cdot 99.52\% = S_b \tag{18}$$

$$V_a \cdot I_a \cdot 99.52\% = V_b \cdot I_b \tag{19}$$

In Equation (20), Equation (19) was solved for the phase current I_{b} on the output side of the LVR. The current ΔI_{LVR} required by the LVR was then calculated from the difference of the two currents, as shown in Equation (21).

$$I_b = \frac{V_a \cdot I_a \cdot 99.52\%}{V_b} \tag{20}$$

$$\Delta I_{LVR} = I_a - I_b \tag{21}$$

The current required by the LVR was taken into account in the balance of the phase currents (step 2) of the next time step. The imputation of the losses was thus time-delayed. In the first time step, the current required by the LVR was not credited. The calculation process for one time step was completed at this point. The results were then saved.

5. Development and Investigation of Different Scenarios

All the scenarios described in the following refer to the low-voltage grid shown in Figure 4. Overall, eight different scenarios were simulated, which differed in terms of the power consumption, the feed-in of the prosumers, and the position of the LVR. The power consumption and feed-in were characterized by the variables $S_{\mathrm{con,k}}$, $S_{\mathrm{pv,k}}$, and $S_{\mathrm{bat,k}}$, defined in chapter 3.2. The position of the LVR was defined by the vector LVR_{pos}, described in step 4 of chapter 4.

The maximum expected power consumption of the prosumers at the end of line k (denoted as $S_{\mathrm{con,k,max}}$in Table 3) was estimated based on the grid data provided by Sundsvall elnät. These data contained the maximum value of the apparent power measured for all the line sections of the grid. The maximum apparent power of a line section that ended at a connection point corresponded to the maximum expected apparent power consumption of the prosumers located there. The scenarios were divided into scenarios with a high and low power consumption. For each prosumer, a constant power consumption was assumed over the simulation period. This corresponded to 70% of the maximum expected apparent power consumption in scenarios with a high consumption and 30% in scenarios with a low consumption.

Table 3. Overview of the simulated scenarios.

		Battery (B)	**Battery + PV (BP)**
Low consumption (L) ($0.30 \times S_{\mathrm{con,k,max}}$)	$LVR_{\mathrm{pos}}(1,2)$	Scenario LB2	Scenario LBP2
	$LVR_{\mathrm{pos}}(1,7)$	Scenario LB7	Scenario LBP7
High consumption (H) ($0.70 \times S_{\mathrm{con,k,max}}$)	$LVR_{\mathrm{pos}}(1,2)$	Scenario HB2	Scenario HB7
	$LVR_{\mathrm{pos}}(1,7)$	Scenario HBP2	Scenario HBP7

With respect to the power output of the PV systems, a distinction was made between scenarios with and without a PV feed-in. In the scenarios with a PV feed-in, a PV generation capacity of 10 kWp was defined for all the prosumers, which corresponded to a typical nominal capacity for the private PV systems. The PV power generation of all the prosumers took place over the entire simulation period with a constant nominal power.

In contrast to the PV feed-in, the delivered power of the FFR capacities varied over the duration of the simulation. It was assumed that the battery capacities were evenly distributed among all the prosumers. The nominal discharge capacity of the battery storage units was sized at 6 kW per prosumer. This represented a standard market size for the battery storage systems with a PV rated capacity of 6 to 10 kW, as shown in the Electricity Storage Inspection 2023 [14]. Furthermore, it was assumed that the total discharge capacity of all the customers was placed on the market by the aggregator as a single bid.

In the synchronous grid of Northern Europe, the activation of the FFR capacities was based on a control that used the utility frequency as a control variable. The provider can choose between three different alternatives for controlling the FFR activation. These differ in terms of the frequency from which the reserve is activated and the maximum permissible activation time [15]. In all the scenarios of the simulation, the alternative B was chosen for the control. Here, the activation took place at a grid frequency of 49.6 Hz, with a maximum activation time of one second. The maximum activation time, which was used for the simulation, was represented by the size of the gap marked with number 1 in Figure 11.

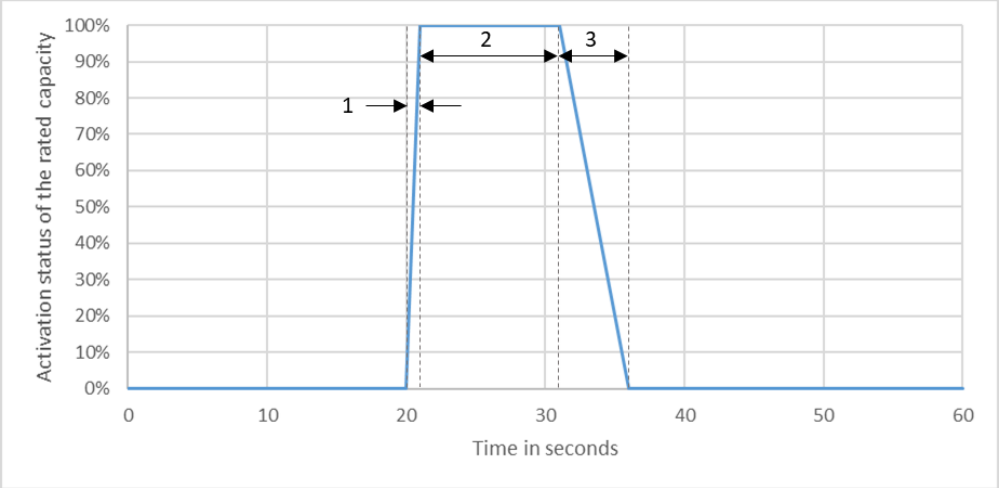


Figure 11. Graph of the FFR signal with activation time (1), support duration (2), and deactivation time (3).

Since the utility frequency is independent of the location, when the activation frequency is reached, there is a simultaneous activation of the reserves of all the prosumers, provided that the bid has been accepted and their batteries are on standby. Regarding the support duration of the FFR, it must be specified by the provider whether it is short (at least 5 s) or long (at least 30 s). During this time, the full FFR capacity must be available [15]. For the activation signal considered here, a short support duration of 10 s was specified. This was intentionally chosen to be longer than the minimum support duration in order to observe any voltage violations that required a duration longer than 5 s. In Figure 11, the support duration is indicated by the length of the arrow marked with number 2.

After the support duration, the reserves are deactivated. The decrease must not exceed 20% of the prequalified FFR per second after a short support time [15]. For the deactivation considered here, a steady deactivation at the maximum deactivation rate was assumed, resulting in a deactivation time of 5 s. It is represented by the length of arrow 3 in Figure 11. The charging process, which must start no earlier than 15 s after the start of deactivation, was not simulated.

The scenarios were also categorized with respect to the position of the LVR. In the default case, the LVR was modeled before the second node, and thus near the beginning of the observed line with index $k = 1$. To test whether deploying the LVR in the middle of the line proved to be more effective, the LVR was modeled before the seventh node in the alternative case.

Table 3 shows an overview of the simulated scenarios. The naming of the scenarios followed a simple naming rule: Scenarios with a low power consumption started with the letter L, while those with a high power consumption started with the letter H. The initial letter was followed by either the letter B or the letter combination BP. The letter B stood for the scenarios in which there was only a feed-in by the FFR reserves. In the scenarios marked with BP, there was an additional PV feed-in. The last digit of the name was associated with the number of the node in front of which the LVR was positioned.

6. Simulation Results and Discussion

6.1. Simulation Results

In the following, the evaluation of all the scenarios for the nodes of the observed line with the LVR took place. The course of the line can be traced in Figure 4. It started at the transformer and ended at node 13 on the top left. All the 13 nodes of the line were examined for short-term voltage deviations and voltage violations. In order to evaluate the effect of the LVR, the scenarios were each evaluated with and without the use of an LVR.

Tables 4–7 compare the duration of the significant exceedances of the reference voltage for the respective affected scenarios. This is indicated by the letter n, which is followed by either the index d or the index v. The index d is added for deviations greater then 10% and the index v is added for deviations greater then 15% of the reference voltage. The following $+$ or $-$ sign indicates whether it is an overvoltage or undervoltage. Another variable is Δt, which represents the total duration of all the deviations occurring at a node. It is important to clarify that the summation of Δt over several nodes, which can be seen on the right side of the tables, resulted in a number that did not represent an actual time span, as the voltage deviations at the different nodes overlapped in time.

Table 4. Number of voltage deviations n_d and violations n_v and their durations Δt for HB2 and HB7.

	Node	**1**	**2**	**3**	**4**	**5**	**6**	**7**	**8**	**9**	**10**	**11**	**12**	**13**	**Σ**
No LVR	n_{d-}	0	0	0	0	0	2	2	2	2	2	2	2	2	16
	Δt_{d-} in s	-	-	-	-	-	44.2	45	45.4	45.6	45.8	45.8	45.8	46.2	363.8
$LVR_{pos}(1,2)$	n_{d-}	0	0	0	0	0	0	0	0	0	0	0	0	0	0
	Δt_{d-} in s	-	-	-	-	-	-	-	-	-	-	-	-	-	0
$LVR_{pos}(1,7)$	n_{d-}	0	0	0	0	0	2	0	0	0	0	0	0	0	2
	Δt_{d-} in s	-	-	-	-	-	44.2	-	-	-	-	-	-	-	44.2

Table 5. Number of voltage deviations n_d and violations n_v and their durations Δt for HBP2 and HBP7.

	Node	**1**	**2**	**3**	**4**	**5**	**6**	**7**	**8**	**9**	**10**	**11**	**12**	**13**	**Σ**
No LVR	n_{d+}	0	0	0	0	1	1	1	1	1	1	1	1	1	9
	Δt_{d+} in s	-	-	-	-	10.8	14.2	15.2	15.4	15.6	60.2	60.2	60.2	60.2	312.0
	n_{v+}	0	0	0	0	0	0	1	1	1	1	1	1	1	7
	Δt_{v+} in s	0	0	0	0	0	0	11.6	12.4	12.8	13.6	13.6	13.6	14	91.6
$LVR_{pos}(1,2)$	n_{d+}	0	0	0	0	0	0	0	1	1	1	1	1	1	6
	Δt_{d+} in s	-	-	-	-	-	-	-	10.6	11.4	12.0	12.4	12.4	12.8	71.6
$LVR_{pos}(1,7)$	n_{d+}	0	0	0	0	1	1	0	0	0	1	1	1	1	6
	Δt_{d+} in s	-	-	-	-	10.8	14.2	-	-	-	10.6	10.8	10.8	11.8	69.0

Table 6. Number of voltage deviations n_d and violations n_v and their durations Δt for LB2 and LB7.

	Node	1	2	3	4	5	6	7	8	9	10	11	12	13	Σ
$LVR_{pos}(1,2)$	n_{d-}	-	-	-	1	1	1	1	1	1	1	1	1	1	10
	Δt_{d-} in s	-	-	-	3.4	4.0	4.4	4.4	4.4	4.6	4.6	4.6	4.6	4.6	43.6
	n_{d+}	-	-	-	-	1	1	1	1	1	1	1	1	1	9
	Δt_{d+} in s	-	-	-	-	4.6	4.8	4.8	4.8	4.8	4.8	4.8	4.8	4.8	43.0
$LVR_{pos}(1,7)$	n_{d-}	-	-	-	-	-	-	1	1	1	1	1	1	1	7
	Δt_{d-} in s	-	-	-	-	-	-	4.8	4.8	4.8	5.0	5.0	5.0	5.0	34.4
	n_{d+}	-	-	-	-	-	-	1	1	1	1	1	1	1	7
	Δt_{d+} in s	-	-	-	-	-	-	4.8	4.8	4.8	4.8	4.8	4.8	4.8	33.6
	n_{v+}	-	-	-	-	-	-	-	-	-	1	1	1	1	4
	Δt_{v+} in s	-	-	-	-	-	-	-	-	-	4.2	4.6	4.6	4.6	18.0

Table 7. Number of voltage deviations n_d and violations n_v and their durations Δt for LBP2 and LBP7.

	Node	1	2	3	4	5	6	7	8	9	10	11	12	13	Σ
No LVR	n_{d+}	-	-	-	-	1	1	1	1	1	1	1	1	1	9
	Δt_{d+} in s	-	-	-	-	14.4	60.2	60.2	60.2	60.2	60.2	60.2	60.2	60.2	496.0
	n_{v+}	-	-	-	-		1	1	1	1	1	1	1	1	8
	Δt_{v+} in s	-	-	-	-		13.2	15	15.6	59.8	60.2	60.2	60.2	60.2	344.4
$LVR_{pos}(1,2)$	n_{d+}	-	-	-	-	-	-	1	1	1	1	1	1	1	7
	Δt_{d+} in s	-	-	-	-	-	-	13.2	14.2	14.8	15.4	15.6	15.6	59.8	148.6
	n_{v+}	-	-	-	-	-	-	-	-	1	1	1	1	1	5
	Δt_{v+} in s	-	-	-	-	-	-	-	-	10.4	12	12.4	12.6	13.6	61.0
$LVR_{pos}(1,7)$	n_{d+}	-	-	-	-	1	1	1	1	1	1	1	1	1	9
	Δt_{d+} in s	-	-	-	-	14.4	60.2	10.2	12.6	13.6	14.4	14.6	14.8	15.2	170.0
	n_{v+}	-	-	-	-	-	1	-	-	-	-	-	1	1	3
	Δt_{v+} in s	-	-	-	-	-	13.2	-	-	-	-	-	10.2	11.8	35.2

These variables enabled a detailed assessment of the effects of different scenarios on the voltage stability and quality within the simulation. By quantifying the deviations at various nodes, it became possible to evaluate and compare the effect of the LVR and its position on voltage performance.

Scenario HB2 and HB7: In both the scenarios, the consistently high consumption resulted in low voltage levels until the FFR capacities were activated. Therefore, the LVR raised the voltage by 8% at the beginning. After the capacities were activated, despite the retention of the 8% increase, the voltage at the end of the line remained within the tolerance range. This can be observed in Figure 12, which depicts the voltage profile over time at node 13 for scenario HB2. This voltage profile was approximately identical for scenario HB7. Shortly after the FFR capacities were activated at t = 20 s, the voltage stayed just below the upper threshold of the tolerance range. After the deactivation of the FFR capacities, the voltage dropped back to its initial value, with the set tap continuing to raise the voltage by 8%, thus keeping it within the tolerance range. Hence, no tap change was observed.

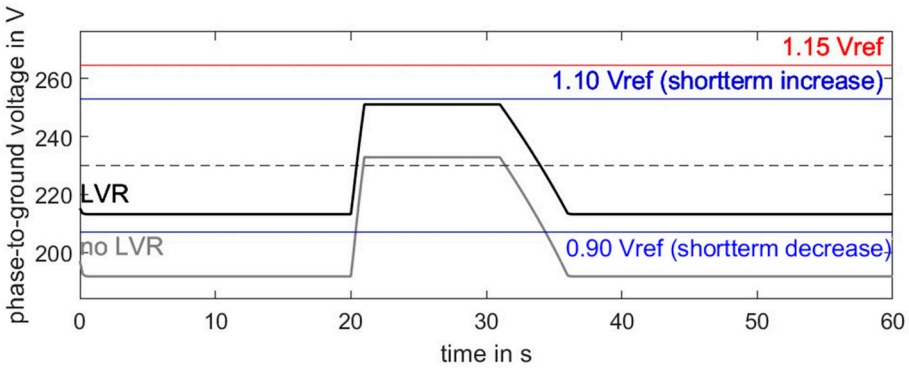


Figure 12. Voltage-over-time profile at node 13 for scenario HB2.

Without the LVR, there were short-term voltage decreases both before and after the FFR activation. This was due to an energy imbalance in both scenarios. The high energy consumption was not compensated by any energy feed-in, if the FFR was not active. These voltage decreases occurred not only at node 13 but had already started from node 6, as evident in Figure 13. This figure illustrates the voltage profile in both the scenarios right before the FFR was triggered, with and without the LVR. It can be concluded that installing the LVR between the sixth and the seventh node in this case resulted in a worse voltage situation. This is because of the voltage deviation at node 6. Since the LVR can only prevent voltage deviations at the following nodes, the LVR cannot prevent the short-term voltage decrease there.

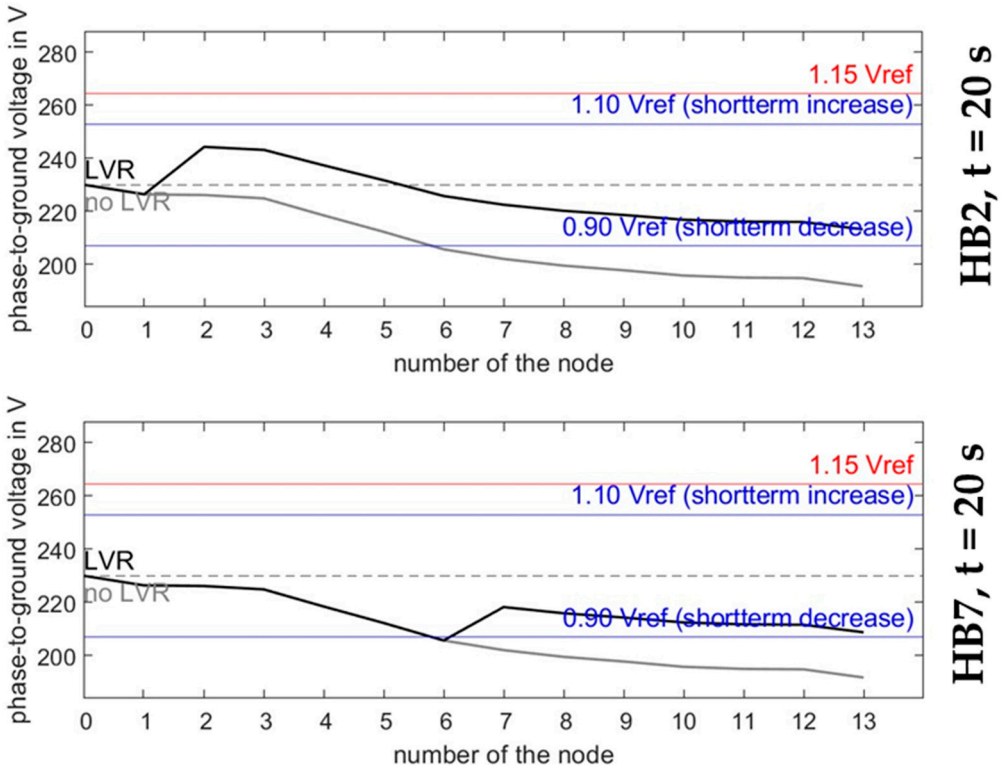


Figure 13. Voltage profile over the nodes of the observed line just before the FFR activation took place for the scenarios HB2 and HB7.

Table 4 compares the voltage deviations in both the scenarios. While in scenario HB2, all the voltage deviations that occurred without the use of the LVR could be prevented, there are two brief voltage deviations lasting a total of 44.2 s at node 6. Apart from this observation, both scenarios were identical in terms of voltage stability.

Scenario HBP2 and HBP7: In this scenario, the LVR reduced the voltage by 8% even before the FFR activation. For scenario HBP7, this can be observed in the voltage profile for node 13, depicted in Figure 14. The graph is again representative of both the scenarios. The reduction was just enough to avoid a voltage violation in both the scenarios, when the FFR reserves were activated. However, the exceedance of the 10% threshold could not be prevented because the LVR was already operating at its maximum voltage reduction. After the deactivation of the FFR, the voltage returned to its original level, with the LVR continuing to reduce the voltage by −8%, bringing the voltage back in the tolerance range. Therefore, there was also no tap change observed in these scenarios.

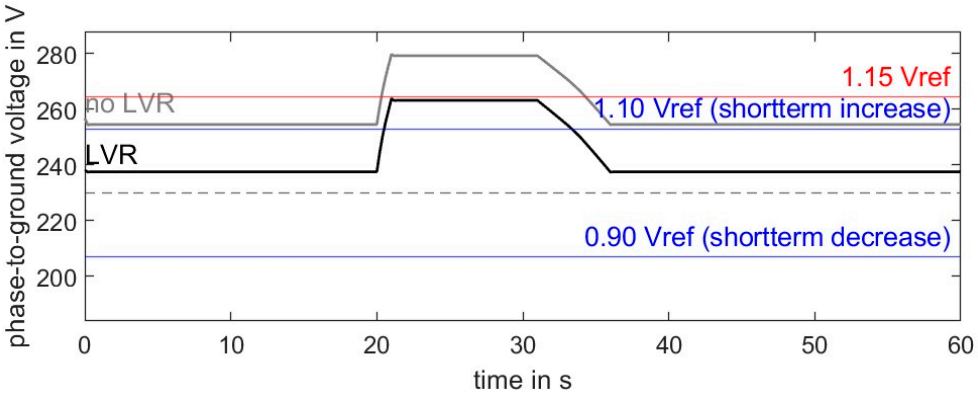


Figure 14. Voltage-over-time profile at node 13 for scenario HBP7.

The reason for the default for the high voltage level was again an energy imbalance. In this case, it was caused by the PV feed-in, which could not be compensated by the high energy consumption, causing high voltages for the entire duration of the simulation.

Without the use of the LVR, the voltage violations would occur starting from the fifth node. This can be observed in Figure 15, which shows the voltage profile along the nodes, captured shortly after the FFR activation. It can be seen that the LVR was able to prevent all the voltage violations, regardless of its installation location. However, the locations of short-term deviations shifted spatially. While in scenario HBP2, they occurred from nodes 8 to 13; nodes 8 and 9 were not affected in scenario HBP7. Instead, due to the shifted position of the LVR, the negative voltage deviations occurred at nodes 5 and 6 in scenario HBP7, as the LVR was located behind these nodes and thus could not prevent the deviations there. In total, six nodes were affected by the voltage deviations in both the scenarios, as shown in Table 5.

However, there was a notable difference: the duration of the individual deviations was distributed more evenly across all the affected nodes in scenario HBP2, while in scenario HBP2, the deviation at node 6 lasted significantly longer than at the other nodes. This could be explained by the fact that the voltage at the end of the line dropped faster after the FFR deactivation than in the middle of the line, where the voltage peak was located in scenario HBP7.

Scenario LB2 and LB7: In scenarios LB2 and LB7, two tap changes could be observed in each case. Before the FFR activation, the voltage was raised by 6% by the LVR. Maintaining this increase resulted in the voltage exceeding the upper threshold of 1.1 V_{ref} after the FFR activation. Subsequently, at t = 25.4 s for LB2 and t = 25.6 s for LB7, there was a tap change from +6.4% to −8% to bring the voltage back in the tolerance range. The following voltage reduction, in turn, caused the voltage to fall below the lower threshold after the deactivation of the FFR capacities. This led to another tap change at t = 39.4 s for LB2 and t = 39.8 s for LB7, to switch from −8% back to +6.4%. For scenario LB2, these voltage changes could be observed for node 13 in Figure 16. The vertical drop or rise in the black LVR line at the specified times reflects the tap changes.

As can be seen in Figure 16, without the use of the LVR, there were no voltage deviations at node 13. This also applied to the voltage at all the other nodes, as shown in Figure 16, which depicts the voltage profiles along the line for both the scenarios. Throughout the simulation duration, there were no short-term voltage deviations at any node without the LVR. In this case, it was evident that under certain conditions, the LVR can cause voltage deviations. These deviations occurred because the LVR slightly raised the voltage from the beginning, leading to an exceedance of the upper threshold upon the FFR activation.

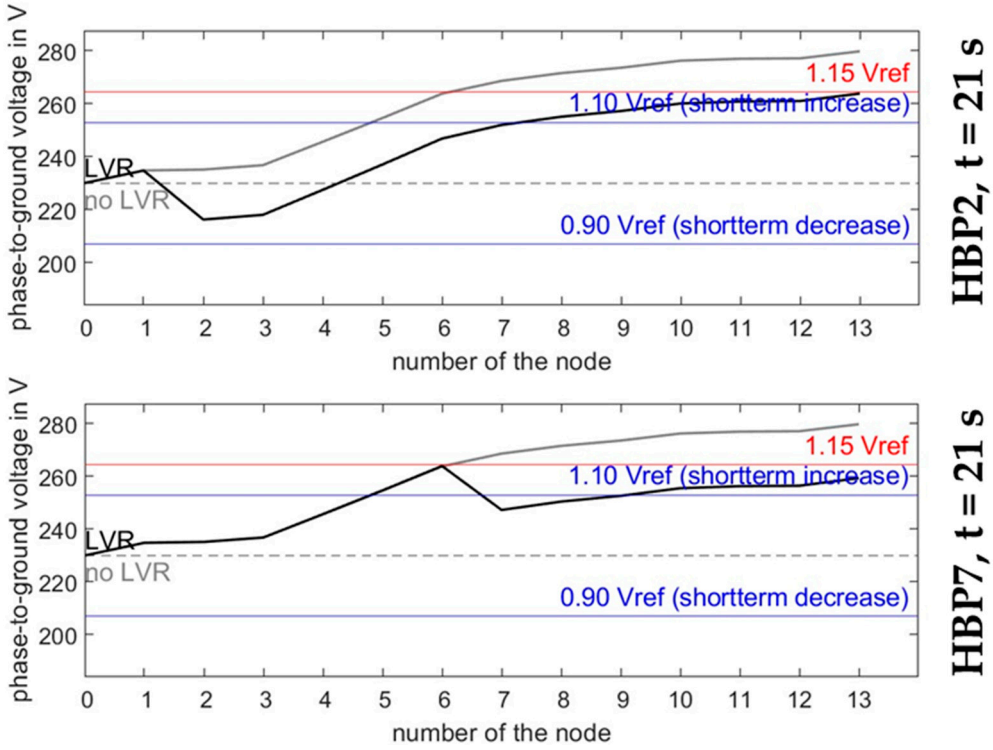


Figure 15. Voltage profile over the nodes of the observed line just after the FFR activation took place for the scenarios HBP2 and HBP7.

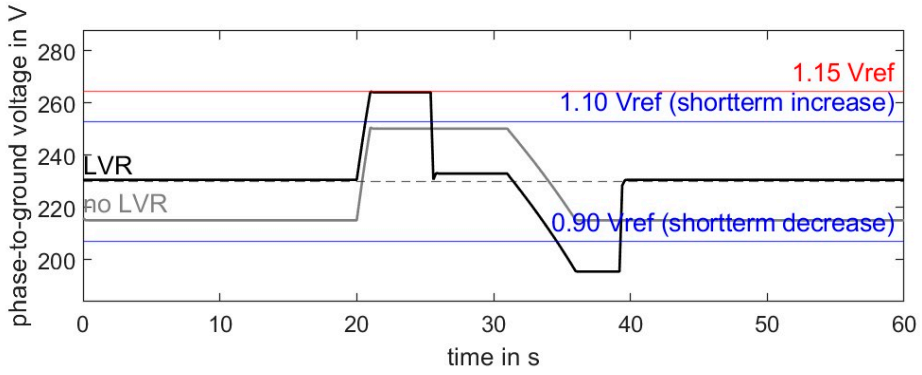


Figure 16. Voltage-over-time profile at node 13 for scenario LB2.

It should be noted that whether these deviations occurred or not, highly depended on the chosen start settings of the tap changer. The start settings, in turn, depended on the preceding events and the corresponding voltage developments in the grid, as explained on page 4. If, for example, the tap selected at the beginning corresponded to a voltage change of 0%, the LVR was not triggered at all.

Figure 16 shows that in scenario LB2, there was no exceedance of V_{ref} by more than 15%. However, this did not apply to scenario LB7, where this threshold was exceeded. Figure 16 was therefore not representative of both cases. In Figure 17, which shows the voltage profile across the nodes shortly after the FFR activation, the differences between LB2 and LB7 can be recognized. The black line in the lower graph is slightly above the red line in scenario LB7, whereas in scenario LB2, it only touches the red line. Table 6 shows that the exceedance in scenario LB7 affects nodes 10 to 13, with the duration of exceedance limited to a maximum of 4.6 s due to the LVR activation. In contrast, the number of nodes affected by the short-term voltage deviations was lower in scenario LB7 compared with scenario LB2.

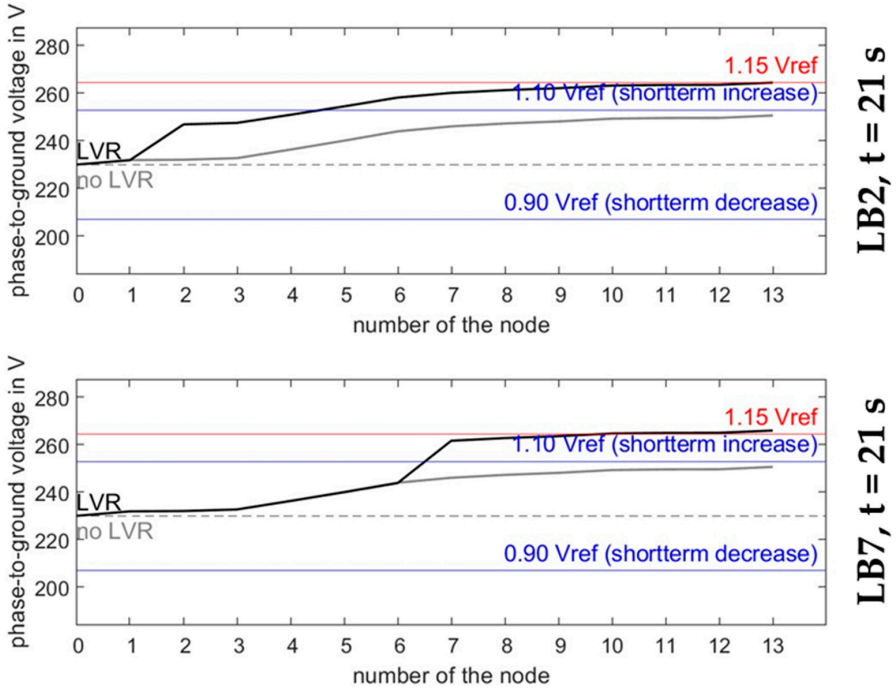


Figure 17. Voltage profile over the nodes of the observed line just after the FFR activation took place for the scenarios LB2 and LB7.

LBP2 and LBP7: In these scenarios, the voltage level was higher than in all the other scenarios. Analogous to HBP2 and HBP7, the LVR reduced the input voltage by 8% over the entire simulation period. However, in the case of LBP2 and LBP7, this reduction was not sufficient to prevent the exceedances of 1.15 V_{ref} that occurred after the FFR activation. Not only did short-term voltage deviations occur, but also voltage violations. For node 13, this can be observed in Figure 18, where the black line exceeds the red line for 13.6 s. After deactivating the FFR capacities, the voltage remained above the threshold for the short-term voltage increases, with the LVR continuing to reduce the voltage by 8%.

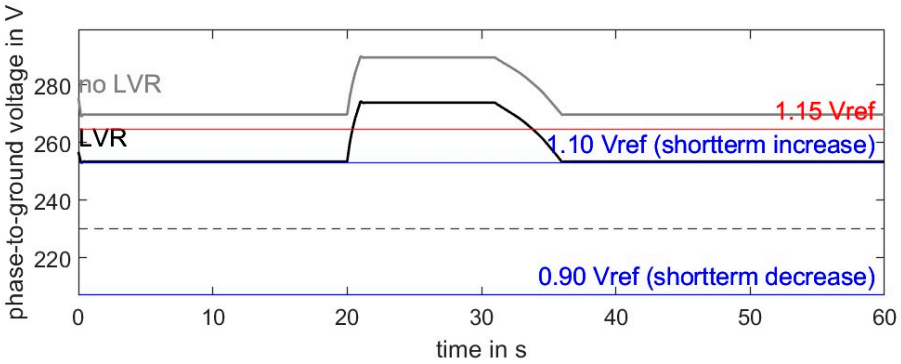


Figure 18. Voltage-over-time profile at node 13 for scenario LBP2.

The reason for the higher voltages, compared with the scenarios HBP2 and HBP7, was due to the lower load. Consequently, the ratio of the generation to consumption was lower, leading to an overall higher voltage level. Thus, despite the set tap of −8%, the voltage could not be reduced sufficiently.

Without the use of the LVR, the voltage remained above the 1.15 V_{ref} throughout the entire duration of the simulation. With the LVR in use, the duration of exceedance was limited to the support duration of the FFR capacities. If this duration exceeded 5 seconds, which was the case in this simulation, it led to voltage violations. These occurred in both scenarios LBP2 and LBP7. However, the installation location was crucial for determining

the number of nodes experiencing voltage violations. Installing the LVR before node 2 resulted in voltage violations at a total of five nodes, whereas installing it before the seventh node resulted in voltage violations at only three nodes. This can be seen in Figure 19 at all nodes, where the black line lies above the red one.

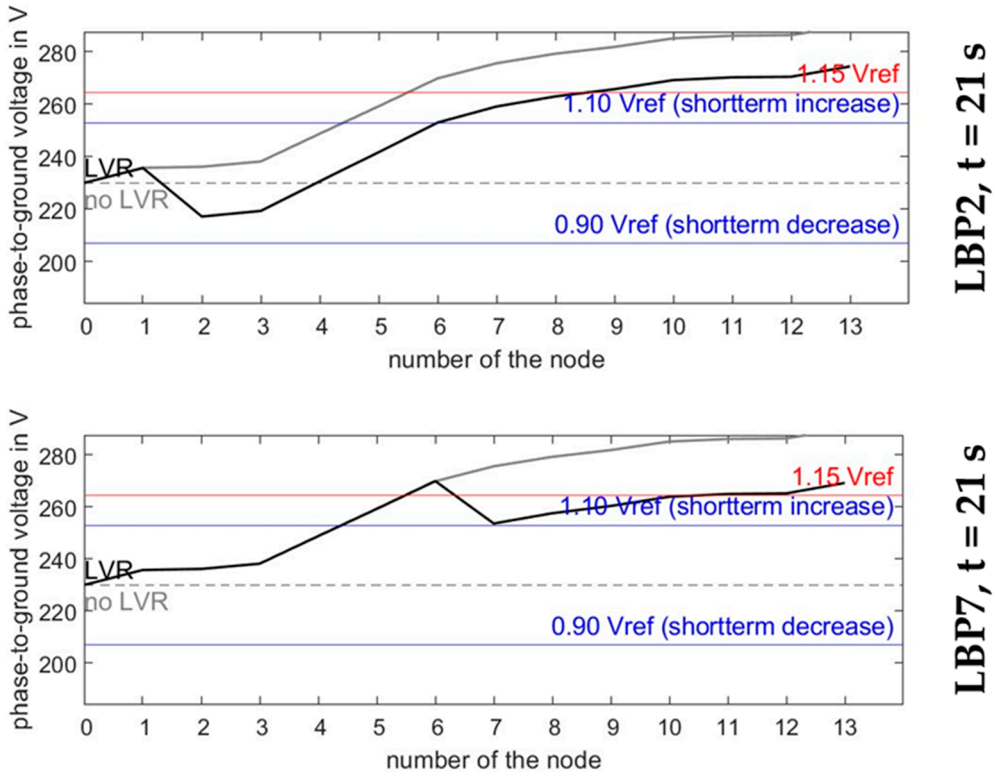


Figure 19. Voltage profile over the nodes of the observed line just after the FFR activation took place for the scenarios LBP2 and LBP7.

Table 7 shows how long the voltage at each node remained in the unauthorized range. Since more violations could be prevented by installing the LVR before the seventh node, this installation location was considered preferable in this scenario.

Comparative analysis: In the following, all the scenarios are briefly compared and the performance of the LVR is evaluated. Therefore, the sum of all the voltage deviations and violations occurring across all nodes and their average duration $\overline{\Delta t}$ is summarized in Tables 8 and 9. Table 8 shows all the scenarios with the LVR installed before the second node and Table 9 with the LVR installed before the seventh node.

Table 8. Number of voltage deviations n_d and violations n_v at all the nodes and their average duration $\overline{\Delta t}$ for the scenarios with the LVR in front of the second node.

Scenario	HB2	HBP2	LB2	LBP2
n_{d-}	0	0	10	0
Δt_{d-} in s	-	-	4.36	-
n_{d+}	0	6	9	7
Δt_{d+} in s	-	11.93	4.78	21.23
n_{v+}	0	0	0	5
Δt_{v+} in s	-	-	-	12.2

Table 9. Number of voltage deviations n_d and violations n_v at all the nodes and their average duration $\overline{\Delta t}$ for the scenarios with the LVR in front of the seventh node.

Scenario	HB7	HBP7	LB7	LBP7
n_{d-}	2	0	7	0
Δt_{d-} in s	22.10	-	4.91	-
n_{d+}	0	6	7	9
Δt_{d+} in s	-	11.50	4.80	18.89
n_{v+}	0	0	4	3
Δt_{v+} in s	-	-	4.50	11.73

The average duration corresponds to the cumulative duration of the deviations or violations at all the affected nodes ($\sum \Delta t$), divided by the number of affected nodes. The number of affected nodes may be smaller than the number of deviations or violations, as one node may be affected by several deviations or violations. Compared with the cumulative duration, the average duration was more suitable for comparison, as it was not dependent on the number of affected nodes.

Regarding Tables 8 and 9, it is noticeable that there were fewer voltage deviations and violations in scenarios with a high load (names starting with an H) than in scenarios with a low load (names starting with an L). This can be explained by the fact that the consumption and generation balanced each other out, which had a mitigating effect on the severity of the voltage surges. In these scenarios, installing the LVR before the second node proved to be more effective, as the two negative voltage deviations with an average duration of 22.10 s could not be prevented in scenario HB7. In scenarios HBP2 and HBP7, where the PV feed-in was taken into account in addition to the high load, deviations occurred at the same number of nodes for both cases, but with the LVR installed in front of the seventh node, the deviations lasted 0.4 s longer on average. This is why the variant with the LVR installed in front of the second node also performed better here.

However, when comparing the scenarios with a low load, the situation was more ambiguous. In the scenarios without PV (LB2 and LB7), for example, three fewer nodes were affected by the positive voltage deviations and two fewer nodes by the negative voltage deviations if the LVR was installed before the seventh node. However, in this case, the voltage violations occurred at four nodes, which did not occur in scenario LB2. As these were not tolerable, the installation location before the second node was the better solution. In the scenarios with PV (LBP2 and LBP7), on the other hand, the position in front of the seventh node performed better. This is because two fewer nodes were affected by the voltage deviations and violations. In addition, the average durations of both the deviations and violations were shorter.

6.2. Discussion

The simulation of the various scenarios showed that the grid voltage rose when the energy fed into the grid predominated and fell when energy consumption predominated. This behavior was expected and suggested that the simulation can at least qualitatively replicate the basic dynamics of a low-voltage grid.

Therefore, it is also reasonable that the voltage deviations exceeding 15% of the reference voltage were observed only in the scenarios characterized by a low electricity demand. If there was also PV generation, the voltage reached such high levels upon the FFR activation that voltage violations could no longer be prevented by the LVR. In the scenario with a low demand and without PV generation, the threshold of 1.15 V_{ref} was also exceeded, but the LVR could prevent voltage violations with the set delay of 5 s. However, these voltage violations only occurred under the assumption that the LVR increased the voltage before the FFR activation.

If the assumptions on the delay and the initial conditions hold true and such a scenario occurred, then the communication between the grid operator and the aggregator was considered reasonable. The aggregator already knew in advance, possibly several days

ahead, whether its capacities will be called upon and at which hours of the day. By transmitting this information to the grid operator, the latter can adjust the regulation for activating the LVR accordingly.

A specific implementation proposal could be as follows: The aggregator sends the network operator an updated list containing the information about the customers on standby for the FFR delivery, their offered power, and their trigger frequency. With this information, the grid operator can anticipate how much the voltage of the affected line will increase upon the FFR activation. The network operator monitors the grid frequency and adjusts the LVR setting when the FFR reserve trigger frequency is reached. In this specific case, this could involve bypassing the LVR or manually adjusting the tap change to a 0% voltage change, as the grid can handle the activation without the LVR.

Another approach could be to use an optimized LVR with a continuous voltage adjustment to eliminate the problem. In a laboratory analysis, a conventional LVR with a stepwise adjustment was compared with a new type of LVR with a continuous voltage adjustment. It was found that an amplification of the voltage fluctuations that occurred with the conventional LVR could be avoided with the novel LVR [9]. If this behavior can be transferred to larger grids, the novel LVR could be a potential solution to the problem.

Regarding the positioning of the LVR, it can be stated that using it in the middle of the line instead of at the beginning of the line does not necessarily lead to more effective voltage maintenance. The reason for this is that the voltage can already deviate significantly from the reference voltage at the nodes before the LVR. Thus, these voltage deviations cannot be controlled, which can be observed by comparing HB2 and HB7. On the other hand, an LVR in the middle of the line can prevent the voltage deviations at nodes in the rear part of the line, which cannot be prevented with an LVR at the beginning. This can be observed by comparing the scenarios LBP2 and LBP7. Therefore, the optimal installation location is probably somewhere in first third of the line. However, this must not be true for the other grids since the optimal installation location depends on the course of the voltage along the affected line.

Grid operators are therefore advised to take voltage measurements at various locations on a line that is affected by voltage fluctuations. For the installation of the LVR, a position should be selected that is as close as possible to the end of the line, but where there are no significant deviations from the reference voltage. If no or not enough voltage measurement points are available, the simulation created can be used to roughly estimate the voltage curve along the affected line. The grid structure, feed-in and consumption data, fuse variables, and line impedances are required as input for this.

It should be noted, however, that although the simulation provides qualitatively plausible results, it is unlikely to exactly match the voltages that would occur in reality. To do justice to the complexity of real power grids, further factors would have to be taken into account. This includes the consideration of an uneven loading of the three phases, which was neglected in this simulation.

Furthermore, the temporal change of external influences, such as the weather, has so far been neglected in this simulation. One effect that could amplify the short-term voltage increases is sudden, local changes in irradiance due to cloud drafts. If such an event and an FFR activation occur simultaneously, the voltages at the nodes could change even faster than in the simulated scenarios. However, to properly represent the local shading effects, the shading must be simulated taking into account the geographic location of the prosumers and therefore the grid topology. Embedding such a shading model in the simulation would be a useful addition to test the effectiveness of the LVR under even more challenging conditions.

7. Conclusions

This study used a simulation to investigate if the voltage regulations in a low-voltage grid can be met with the help of an LVR. The fundamental assumption was that the cumulative discharge capacity of future private battery storage systems will be offered

as an FFR via aggregators. The expansion of private battery storage was assumed to go hand-in-hand with the expansion of the PV systems.

With the current mode of operation and position of the LVR, violations of the voltage regulations can occur. This happens when the total power drawn from the grid is low and when there is a simultaneous feed-in of the PV- and FFR-capacities. The resulting voltage increases cannot be sufficiently compensated by the LVR to keep the voltage within the permissible voltage range.

If only the FFR capacities feed into the grid and the electricity consumption of the customers is low, then the use of the LVR leads to voltage deviations, if it has already increased the voltage before the FFR activation. This is because after the activation, the voltage continues to be raised until the next tap change occurs. During this period, the additional voltage increase caused by the LVR results in deviations that would not occur without the LVR. This does not constitute a voltage violation solely because the duration of the exceedance is very short. However, the duration of the exceedance depends greatly on the assumed time delay of the LVR. If the set delay is greater than the assumed 5 s, voltage violations could also occur in this scenario. To mitigate the voltage surge amplification caused by the LVR, the following procedure is recommended:

1. Establishing communication between the distribution system operator and the aggregator.
2. The aggregator informs the distribution system operator about the standby times of capacities.
3. The grid operator adjusts the operating mode of the LVR accordingly during this period.

A comparison of the positions of the LVRs considered has shown that both variants have weak points. In some cases, an LVR located at the beginning of the line cannot prevent as many overvoltages at the end of the line as an LVR positioned further back. However, if the LVR is too close to the end of the line, voltage deviations can occur upstream of the LVR, which can therefore no longer be controlled. To identify the best location for the LVR, grid operators are recommended to carry out voltage measurements along the affected line and select the location taking the following two criteria into account:

- The installation location of the LVR should not be behind a node where voltage deviations are already occurring.
- In compliance with the first criterion, the distance between the LVR and the end of the line should be minimized.

However, if no measuring points are available, the simulation created in this work can be used as a rough estimate of the voltage profile. This requires information on the grid structure, the impedances of the lines, the voltage values, and the feed-in and consumption behavior of the prosumers. For a more precise calculation of the voltage profile of the affected line, the simulation must better reflect the complexity of real low-voltage grids. In order to improve the simulation, the implementation of the following aspects is recommended, for example as part of subsequent work:

- Consideration of the asymmetric phase feeding and loading by the prosumers connected to the grid.
- Consideration of local changes in the radiation intensity due to cloud cover, taking into account the grid topography.

To summarize, it can be stated that the developed simulation works and can reproduce the basic dynamics of the considered low-voltage grid qualitatively well. The extent to which the simulation can be optimized to accurately represent real voltage conditions could be the subject of future research. In particular, we consider a comparative analysis of a simulated and a measured voltage profile in a low-voltage grid to be interesting.

Author Contributions: Conceptualization, K.B.; Methodology, M.H.; Software, M.H. and K.B.; Validation, M.H.; Formal analysis, M.H.; Investigation, M.H.; Writing—original draft, M.H.; Writing—review & editing, K.B.; Supervision, K.B.; Project administration, K.B. All authors have read and agreed to the published version of the manuscript.

Funding: This research received no external funding.

Data Availability Statement: The data will be provided on request.

Acknowledgments: Throughout this project, we maintained a continuous exchange with the grid operator, Sundsvall elnät AB. They generously provided us with data on their distribution grid, which we utilized to model it in Matlab. Furthermore, they offered valuable assistance by promptly addressing all questions that emerged during the course of our work regarding the distribution grid and the LVR in use. We are grateful to Sundsvall elnät for their excellent cooperation.

Conflicts of Interest: The authors declare no conflicts of interest.

References

1. Al-Shetwi, A.Q.; Hannan, M.A.; Jern, K.P.; Mansur, M.; Mahlia, T.M. Grid-connected renewable energy sources: Review of the recent integration requirements and control methods. *J. Clean. Prod.* **2020**, *253*, 119831. [CrossRef]
2. European Parliament and European Council. Regulation (EU) 2019/943 of the European parliament and of the council of 5 June 2019 on the internal market for electricity. *Off. J. Eur. Union* **2019**, *158*, 54–124.
3. Zakeri, B.; Gissey, G.C.; Dodds, P.E.; Subkhankulova, D. Centralized vs. distributed energy storage e Benefits for residential users. *Energy* **2021**, *236*, 121443. [CrossRef]
4. Gomez-Gonzalez, M.; Hernandez, J.C.; Vera, D.; Jurado, F. Optimal sizing and power schedule in PV household-prosumers for improving PV self-consumption and providing frequency containment reserve. *Energy* **2020**, *191*, 116554. [CrossRef]
5. Ström, L.; Bollen, M.; Kolessar, R. Voltage quality regulation in Sweden. In Proceedings of the CIRED 21st International Conference on Electricity Distribution 2011, Frankfurt, Germany, 6–9 June 2011; pp. 1–4.
6. Bhosale, G.; Vakhare, A.; Kaystha, A.; Aher, A.; Pansare, V. Overvoltage, undervoltage protection of electrical equipment. *Int. Res. J. Eng. Technol. (IRJET)* **2018**, *2*, 29–32.
7. Morén, G. Energimarknadsinspektionens författningssamling. *Swed. Energy Mark. Insp. (Ei)* **2013**, *1*, 1–7.
8. Holt, M.; Maasmann, J.; Rehtanz, C. Line voltage regulator based on magnetic controlled inductors for low-voltage grids. *CIRED-Open Access Proc. J.* **2017**, *2017*, 278–281. [CrossRef]
9. Holt, M.; Rehtanz, C. Optimizing line-voltage-regulators with regard to power quality. *Electr. Power Syst. Res.* **2021**, *190*, 106654. [CrossRef]
10. Hartung, M.; Baerthlein, E.; Panosyan, A. Comparative study of tap changer control algorithms for distribution networks with high penetration of renewables. In *CIRED Workshop*; CIRED: Rome, Italy, 2014; pp. 1–5.
11. Holt, M.; Grosse-Holz, G.; Rehtanz, C. Line voltage regulation in low voltage grids. In *CIRED Workshop*; CIRED: Ljubljana, Slovenia, 2018; pp. 1–4.
12. Hitachi Energy. Line voltage regulator for low-voltage grids. In *Public Brochure DEABB 5154 15 en*; Hitachi Energy: Singapore, 2022; pp. 1–2.
13. Filipović, Ž. Energieversorgung elektrischer Bahnen. In *Elektrische Bahnen*, 5th ed.; Springer Vieweg: Berlin/Heidelberg, Germany, 2015; Volume 5, pp. 257–272.
14. Weniger, J.; Orth, N.; Meissner, L.; Schlüter, C.; Meyne, J. *Energy Storage Inspection 2023*; HTW: Berlin, Germany, 2019; pp. 1–50.
15. ENTSO-E. *Technical Requirements for Fast Frequency Reserve Provision in the Nordic Synchronous Area*; External Document 2021, Version 1.1; HTW: Berlin, Germany, 2023; pp. 1–16.

Disclaimer/Publisher's Note: The statements, opinions and data contained in all publications are solely those of the individual author(s) and contributor(s) and not of MDPI and/or the editor(s). MDPI and/or the editor(s) disclaim responsibility for any injury to people or property resulting from any ideas, methods, instructions or products referred to in the content.